

Outlier Detection in the DESI Bright Galaxy Survey

YAN LIANG ¹ PETER MELCHIOR ^{1,2} CHANGHOON HAHN ¹ JEFF SHEN ¹ ANDY GOULDING ¹ AND
CHARLOTTE WARD ¹

¹*Department of Astrophysical Sciences, Princeton University, Princeton, NJ 08544, USA*

²*Center for Statistics & Machine Learning, Princeton University, Princeton, NJ 08544, USA*

ABSTRACT

We present an unsupervised search for outliers in the Bright Galaxy Survey (BGS) dataset from the DESI Early Data Release. This analysis utilizes an autoencoder to compress galaxy spectra into a compact, redshift-invariant latent space, and a normalizing flow to identify low-probability objects. The most prominent outliers show distinctive spectral features such as irregular or double-peaked emission lines, or originate from galaxy mergers, blended sources, and rare quasar types, including one previously unknown Broad Absorption Line system. A significant portion of the BGS outliers are stars spectroscopically misclassified as galaxies. By building our own star model trained on spectra from the DESI Milky Way Survey, we have determined that the misclassification likely stems from the Principle Component Analysis of stars in the DESI pipeline. To aid follow-up studies, we make the full probability catalog of all BGS objects and our pre-trained models publicly available.

Keywords: galaxies: statistics – techniques: spectroscopic

1. INTRODUCTION

Large spectroscopic surveys, such as the Sloan Digital Sky Survey (SDSS; York et al. 2000), have gathered spectroscopic data for millions of astronomical objects. The next generation of surveys, such as the Dark Energy Spectroscopic Instrument (DESI; DESI Collaboration et al. 2016), produce even larger datasets. While the majority of cataloged objects can be classified using known spectral types, there also exist “unknown unknowns”—rare phenomena or object types that deviate from established physical models. In such cases, unsupervised machine learning methods can identify features in the data without relying on predefined labels or pre-determined templates. Such methods are particularly valuable for detecting outliers, which are, by definition, rare and often unexpected.

In this work, we search for outliers in the Early Data Release (EDR; DESI Collaboration et al. 2023a) of the DESI Bright Galaxy Survey (BGS; Hahn et al. 2023), which we briefly describe in Section 2. We employ the spectrum autoencoder (AE) architecture SPENDER introduced by Melchior et al. (2022). This technique com-

presses galaxy spectra into a compact, redshift-invariant latent space, representing the “type” of galaxies, and makes full use of the observed spectra across all redshifts. Following the approach of Liang et al. (2023), we interpret the sample density in the AE latent space as a probability distribution, and identify outliers as low-probability objects using a normalizing flow (NF) model. We describe this approach in Section 3.

Our previous application of this method to SDSS galaxy spectra uncovered a range of astrophysical and instrumental outliers, including blends of multiple galaxies and/or stars, extremely reddened galaxies, as well as stars that had been misclassified as galaxies (Liang et al. 2023). With the new DESI dataset, we again expect outliers to correspond to galaxies in unusual physical states. We also expect them to reveal failures or artifacts of the data processing pipelines and therefore serve as an alternative mechanism for quality control, sensitive to problems that were not even known to be problems.

In Section 4, we present and discuss the nature of remarkable outliers in the BGS galaxy sample, including merging galaxies and rare quasars. Our visual inspection also reveals a substantial fraction to be misclassified stars. In Section 5, we extend our generative modeling approach to stellar spectra from the DESI Milky Way Survey (MWS; Cooper et al. 2023), and identify

the likely reason why some BGS galaxies were misclassified. We conclude in Section 6 with a discussion of the limitations and potential extensions of this study.

2. DATA

We use data from the DESI EDR, which includes spectra observed during the Survey Validation (SV) campaign that was conducted before the start of the main survey to evaluate DESI’s scientific program (DESI Collaboration et al. 2023b). SV was divided into two main phases: an initial ‘Target Selection Validation’ phase to finalize the target selection and a pilot survey of the full DESI program that covered $\sim 140 \text{ deg}^2$, the One-Percent Survey.

In this work we focus on targets from the BGS and the MWS. The initial target lists are defined on the basis of the imaging data from the Legacy Surveys (LS; Dey et al. 2019). An object is considered a BGS target if it is either not in the *Gaia* Data Release 2 catalog (Gaia Collaboration et al. 2018) or if it is in *Gaia* and has $(G_{Gaia} - r_{\text{raw}}) > 0.6$, where G_{Gaia} is the G -band magnitude from *Gaia* and r_{raw} is the LS r -band magnitude without galactic extinction correction. Afterwards, a fiber-magnitude cut is imposed to remove imaging artifacts or other spurious objects. Quality cuts then remove any object without photometric observations in all three LS optical bands and with colors outside $-1 < (g - r) < 4$ and $-1 < (r - z) < 4$. Very bright objects with $r > 12$ and $r_{\text{fibertot}} < 15$ are also removed from the sample. For further details on the BGS target selection, see Hahn et al. (2023).

MWS targets consists of objects that are in both LS and *Gaia* Early Data Release 3 (Gaia Collaboration et al. 2021). They are restricted to objects that are classified as point sources based on their morphology and within the magnitude limits $16 < r < 19.2$ and $r_{\text{raw}} < 20$. There is an additional cut on *Gaia* astrometric excess noise (*Gaia* AEN < 3) as well as quality cuts on the the LS g and r -band photometry. No quality cuts on z -band photometry are imposed. For further details on the MWS target selection, see Cooper et al. (2023).

All spectra in the EDR are reduced using the ‘fuji’ version of the DESI spectroscopic data reduction pipeline (Guy et al. 2023). First, spectra are extracted from the spectrograph CCDs using the *spectroperfectionism* algorithm of Bolton & Schlegel (2010). Then, fiber-to-fiber variations are corrected by flat-fielding, and a sky model, empirically derived from sky fibers, is subtracted from each spectrum. Afterwards, the fluxes in the spectra are calibrated using stellar model fits to standard stars. The calibrated spectra are co-added across exposures to produce the final processed spectra. Among the differ-

ent co-adds in the EDR, we use the ones produced by combining all available spectra for a given target.

For each spectrum, the DESI EDR provides redshift measurements from the *Redrock*¹ redshift fitting algorithm. For a given spectrum, *Redrock* derives redshift by minimizing the χ^2 between the observed spectrum and a model spectrum constructed from a linear combination of Principal Component Analysis (PCA) basis spectral templates in three template classes (“stellar”, “galaxy”, and “quasar”). The redshift and template class that produces the lowest χ^2 is used as the best-fit redshift and spectral classification. *Redrock* also provides an estimate of redshift uncertainties, ZERR, and a redshift confidence measurements, $\Delta\chi^2$, which corresponds to the difference between the χ^2 values of the best-fit model and the next best-fit model.

For BGS, we only use spectra observed with functioning fiber positioners and with reliable redshift measurements as defined in Hahn et al. (2023). We only keep spectra classified as galaxy spectra by *Redrock* (i.e. SPECTYPE=="GALAXY") with redshifts $z \in [0, 0.8]$ (cutting off a very minor high-redshift tail) and having no *Redrock* warning flags ZWARN. From MWS, we select spectra with ZWARN==0 and SPECTYPE=="STAR".

With those cuts, we compile approximately 250,000 BGS and 210,000 MWS spectra. The observed wavelength range is $\lambda_{\text{obs}} = 3600 \dots 9824 \text{ \AA}$. We split the samples into training, validation, and testing sets, each accounting for 70%, 15%, and 15% of the entire samples, respectively. We apply a mask to the top ~ 100 telluric lines, assigning zero weights to all bins within 5 \AA of the lines centers, which amounts to approximately 25% of the data vectors. The spectra are then normalized by the median flux over the rest-frame wavelengths $\lambda_{\text{rest}} = 5300 \dots 5850 \text{ \AA}$, a region that is relatively quiescent and accessible at all redshifts, thereby avoiding redshift-dependent encoding.

3. METHODS

Our general approach follows Liang et al. (2023) and is summarized in Figure 1. In short, we train the spectrum autoencoder architecture SPENDER (Melchior et al. 2022) on the observed BGS spectra. That means, we encode a spectrum $\mathbf{x} \in \mathbb{R}^M$ into a small number of latent variables $\mathbf{s} \in \mathbb{R}^S$. For this work, we set $S = 6$. From these latents, the decoder produces a restframe model \mathbf{x}' , which is redshifted and resampled to produce an observed-frame reconstruction \mathbf{x}'' that matches the observation. In the first training phase, we adjust the network weights so as to minimize the fidelity loss, which

¹ <https://redrock.readthedocs.io>

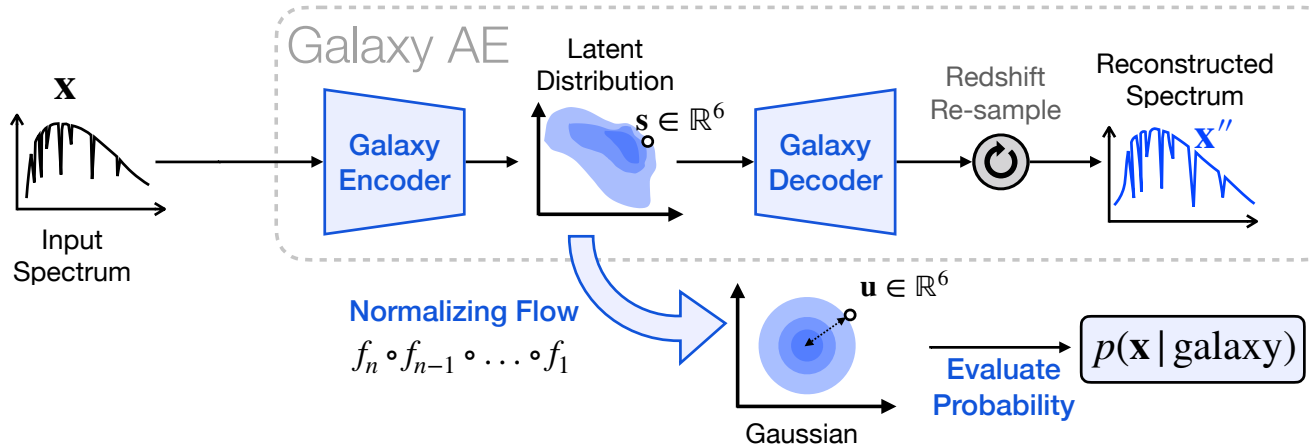


Figure 1. Our approach combines an autoencoder (AE) for spectrum reconstruction and a normalizing flow (NF) for probability estimation. The AE compresses an observed galaxy spectrum into a low-dimensional latent representation of the restframe spectrum, and the NF transforms the latent distribution of the entire BGS galaxy sample into a Gaussian base distribution for efficient probability computation and sampling.

quantifies the reconstruction quality over batches of N spectra:

$$L_{\text{fid}} = \frac{1}{2NM} \sum_i^N \mathbf{w}_i \odot (\mathbf{x}_i - \mathbf{x}_i''(\mathbf{x}_i, z_i))^2, \quad (1)$$

where z_i is the known redshift of source i , \mathbf{w}_i is the inverse variance vector, and \odot the element-wise multiplication. For Gaussian-distributed noise, this loss measures the mean log-likelihood of data given the autoencoder model.

In the second phase, we train with the fidelity loss and two extra losses that make the latent space distribution approximately redshift-invariant. This property yields a more physically meaningful latent distribution and has proven effective for finding outliers in SDSS spectra (Liang et al. 2023). The first extra loss term ensures that spectra that are close in data space are also close in latent space; the second one promotes proximity in latent space between the original spectrum and an augmented version, where we modified the redshift and added additional noise to the spectrum.

Upon convergence of our two-phase training, we achieved fidelity losses of 0.384, 0.391, and 0.386 on the training, validation, and test sets, respectively. The consistency across different datasets indicates that our model is generalizing well on unseen datapoints, with no evidence of significant overfitting. The achieved fidelity corresponds to a reduced chi-square (χ^2) value of 0.77. Figure 2 presents the reconstructed restframe models for three representative galaxy spectra in BGS. As intended, the model also exhibits redshift invariance. In the latent space of the trained auto-encoder model, original spectra and their artificially redshifted augmentation spectra are on average 21 times closer to each

other than the average pairwise distance between different objects. This indicates that our model successfully captures the intrinsic characteristics of galaxies, regardless of their redshift.

As last step, we train a specific type of normalizing flow (NF; Tabak & Vanden-Eijnden 2010; Tabak & Turner 2013) model known as a Masked Autoregressive Flow (MAF; Papamakarios et al. 2017) to describe the density of galaxies in the autoencoder latent space. The combination of an AE and a NF is synergistic: The NF provides a flexible density estimator for the complex latent distributions AEs tend to form, while the AE serves as a non-linear compression scheme to provide a lower-dimensional space for the NF to operate in. Because of our extended training procedure, the latents are approximately invariant under changes of redshift, rendering them much more informative conditioning variables to describe intrinsic galaxy properties than the observed spectrum data vector. With the AE-NF combination, we can evaluate the probability $p_{\text{galaxy}} = p(\mathbf{x} | \text{BGS})$ of any spectrum \mathbf{x} to be drawn from the BGS sample. Spectra with low p_{galaxy} can thus be interpreted as outliers in the galaxy sample.

4. BGS OUTLIERS

We define an outlier score as $-\log p_{\text{galaxy}}$ and visually investigate the top 200 outliers. Figure 3 shows a selection of them. A large fraction contain irregularly-shaped or double-peaked narrow emission lines (e.g. outlier 9², shown in the 2nd row of Figure 3), indicating that the spectra contain overlapping galaxies in cluster

² DESI 39627794417717430

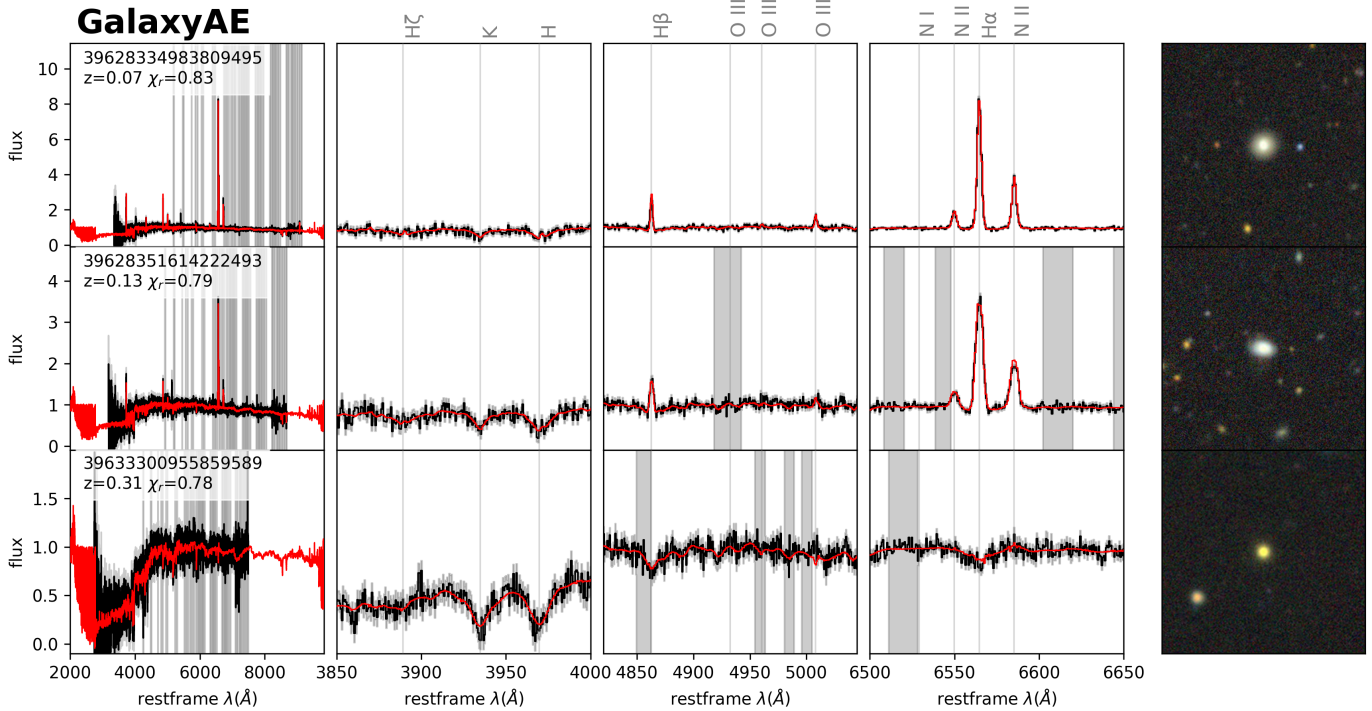


Figure 2. BGS galaxy spectra (black) and their reconstructed models (red) as determined by our spectrum autoencoder. The first column presents the entire flux-normalized restframe spectrum, assuming the *Redrock* redshift, with greyed out regions being masked during training. The second, third, and fourth columns provide zoomed-in views of significant emission/absorption lines. The final column shows the image of the source from the DESI Legacy Imaging Surveys.

environments or galaxy mergers. Outlier 20³ is reported as a galaxy merger in De Propriis et al. (2007), outlier 11⁴ is an ultraluminous infrared galaxy in a merger (Kim et al. 2002) with prominent polycyclic aromatic hydrocarbon (PAH) emission (Lai et al. 2020), and outliers 59⁵ and 60⁶ also have morphologies consistent with a merger. Outliers 4⁷, 43⁸, 51⁹, 91¹⁰, 107¹¹, 125¹², 133¹³, 135¹⁴ and 191¹⁵ have double-peaked narrow emission lines. Double-peaked narrow emission lines can arise due to complex kinematics in the narrow-line region surrounding a single AGN induced by outflows or disk rotation, or the presence two separate narrow-line regions associated with two merging AGN at small relative ve-

locities (Shen et al. 2011). In the cases of 107 and 125, there is a galaxy merger visible in imaging data, but the others have settled galaxy morphologies and no obvious mergers, making them candidates for close separation dual AGN in the late stages of merger. Outlier 151¹⁶ has a triple-peaked narrow line due to a cluster environment apparent in imaging data.

A fraction of the top 200 outliers are reported as dusty, obscured and/or radio-loud AGN in the literature, including outlier 60¹⁷ (Kozieł-Wierzbowska et al. 2020), 69¹⁸ (Chen et al. 2018), and 84¹⁹ (Best & Heckman 2012). Outlier 69 has previously been classified as a Wolf-Rayet galaxy due to detectable emission line features from a large population of Wolf-Rayet stars (Chen et al. 2018). Outlier 37²⁰ was reported on the Transient Name Server (Nordin et al. 2020) due to the detection of AGN-like optical variability in time-domain imaging from the Zwicky Transient Facility (Bellm et al. 2019; Graham et al. 2019).

³ DESI 39627788356946460

⁴ DESI 39627896888755461

⁵ DESI 39628362636858151

⁶ DESI 39633407830920247

⁷ DESI 39633149726034475

⁸ DESI 39633402051166367

⁹ DESI 39627782338122510

¹⁰ DESI 39627794400937953

¹¹ DESI 39633127701745009

¹² DESI 39627800390405432

¹³ DESI 39633154075526488

¹⁴ DESI 39633419134568709

¹⁵ DESI 39627781759307042

¹⁶ DESI 39627746069975548

¹⁷ DESI 39633407830920247

¹⁸ DESI 3962776273159194

¹⁹ DESI 39628334988006041

²⁰ DESI 39627734065874069; TNS AT2020dig

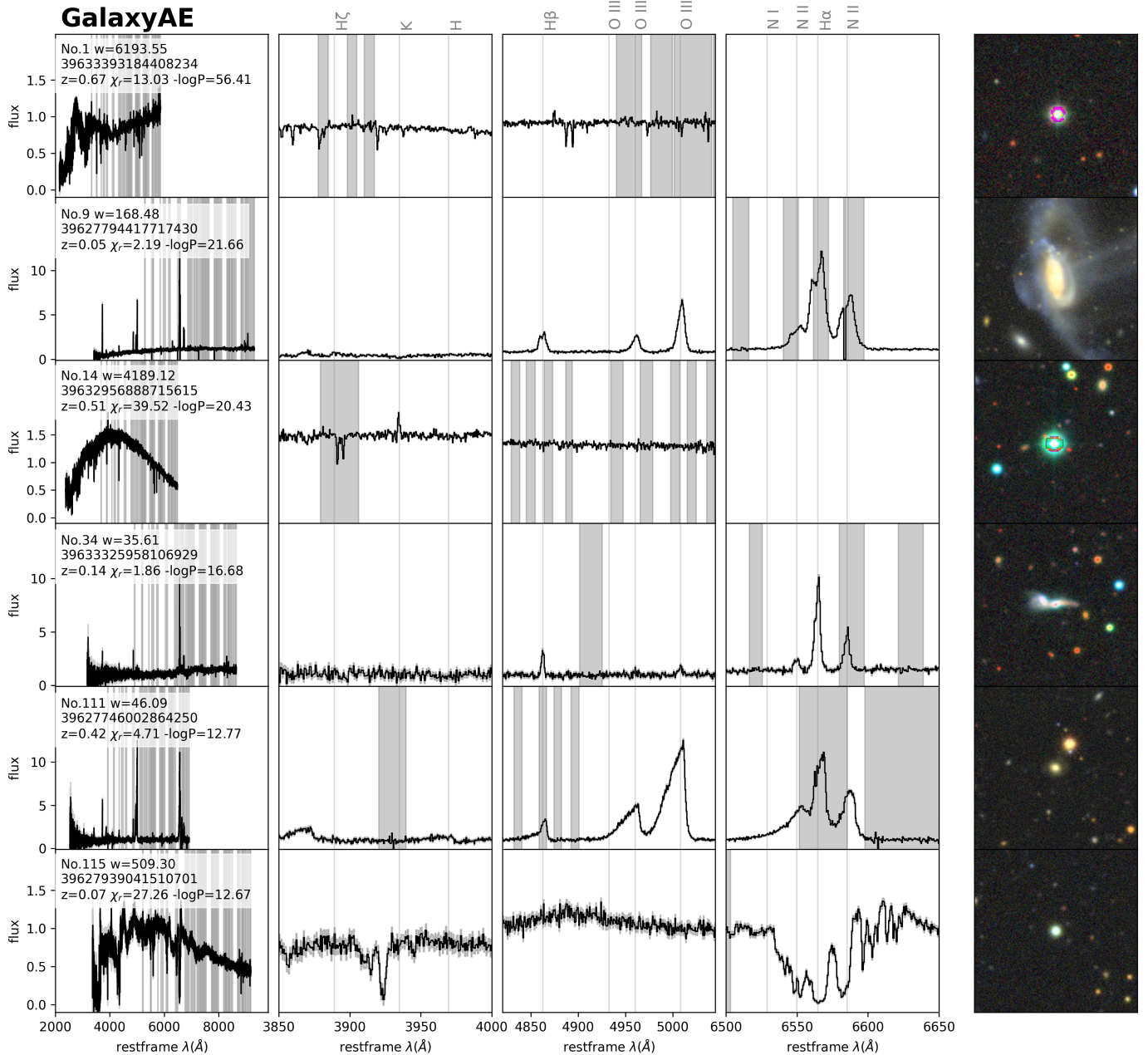


Figure 3. Representative selection of outliers in BGS identified by the galaxy autoencoder and normalizing flow, in decreasing order of the outlier score (details for each object in Section 4). The panels are identical to Figure 2, but for visual clarity we omitted showing the AE model. The legend in the upper left corner includes the DESI Target ID, *Redrock* redshift, reduced chi-square of the AE model, and the negative log probability of the NF model.

Previously unreported, outlier 111²¹ (5th row in Figure 3) has unusually blue-skewing emission lines indicating the presence of high-velocity outflows, similar to those observed in extremely red quasars (ERQs; Ross et al. 2015; Zakamska et al. 2016). Although this ob-

ject’s broad-band color $r - W4 = 18.96 - 6.744 = 12.22$ is not quite as extreme as required by these earlier works ($r - W4 > 14$, where W4 refers to the Vega magnitude in the WISE W4 filter), it is also fainter and towards the low end of the redshift range covered earlier. In any case, line shapes and photometric properties suggest strongly accelerated gas with high levels of dust obscuration or reprocessing in the interstellar medium of the host.

²¹ DESI 39627746002864250

Also previously unknown, outlier 115²² (last row in Figure 3) has complex and broad absorption features. With the *Redrock* redshift estimate of $z = 0.0698$, the H α region would be highly unusual. However, we believe that this source is in fact a Broad Absorption Line (BAL; Hall et al. 2002) quasar at $z = 1.535$, showing MgII λ 2800, CIII λ 1909, and CIV λ 1549 absorption that removes almost all flux directly blueward of the nominal line centers. If true, it demonstrates the ability to search for these highly unusual quasars in DESI BGS at fainter luminosities than were accessible in SDSS.

We also find a variety of blended objects, similar to SDSS galaxy outliers we reported in Liang et al. (2023). Outliers 8²³, 12²⁴, 21²⁵, and 53²⁶ are each consistent with a superposition of two stars. Outlier 34²⁷ (4th row in Figure 3) shows a chance alignment of an M-type star and a distant galaxy merger at $z = 0.13$. Outlier 26²⁸ are multiple galaxies, and outlier 15²⁹ is a pair of quasars.

However, among the top 200 outliers in the BGS galaxy sample, the largest group consists of 35 stars, including outlier 1³⁰ (1st row of Figure 3). Like outlier 14³¹ (3rd row of Figure 3), they often show no indication of blending and are bright enough to reveal the diffraction spikes and saturate the LS images. We suspect that their brightness led to biases in the imaging measurements, including the estimation of size, which made these object appear extended and thus targeted in BGS. What surprises us is that *Redrock* classified these sources as galaxies with sufficient confidence (DELTA $\chi^2 > 40$), sometimes even placing them at cosmological redshifts.

5. STELLAR SPECTRUM MODEL

We further investigate the stellar contamination in the galaxy sample. A closer inspection of these stellar outliers shows that *Redrock* finds a plausible fit with its galaxy PCA templates, but shows larger residuals for its star templates (see Figure 4). These residuals resemble the prominent metal oxide (TiO, VO) absorption features in M dwarfs, but the residuals flip sign in different sources. As these features cannot arise in emission, we surmise that either the mean PCA spectrum or the

eigenvectors *Redrock* uses for its star fits were trained with an overabundance of M dwarfs, so that these metal oxide bands get imprinted on the models of other stars.

To test this hypothesis we make our own star model by following the generative modeling approach of Section 3 and repeat the autoencoder and NF training with stars in the DESI MWS. The typical quality of the StarAE reconstructions of a representative selection of MWS stars can be seen in Figure 5. We also include the StarAE model in Figure 4, demonstrating that it is not affected by the spurious features of the PCA model. We conclude that SPENDER successfully deals with the diversity in stellar types, variations in radial velocity, and observational imperfections, and produces an accurate model that is not limited to a linear combination of orthogonal templates.

We also repeat the training for a NF on the MWS latent distribution to find additional outliers in the BGS sample, following the suspicion that certain targets do not conform neatly to either star or galaxy class. For example, outliers 5³², 22³³, and 23³⁴ are confirmed quasars (Lyke et al. 2020; Véron-Cetty & Véron 2010), while outlier 324³⁵ has been identified as a BL Lac object by Ramazani et al. (2017). Calibration issues, with either a single arm missing or different arms being improperly aligned (e.g. for outliers 4³⁶, 10³⁷, and 31³⁸), can also cause low probability estimates from both flow models.

6. DISCUSSION AND CONCLUSIONS

In this work, we have identified and cataloged outliers from the DESI BGS with a spectrum autoencoder and a normalizing flow. The overall high quality of DESI spectra allows us to present a rich collection of objects exhibiting unusual physical properties, ranging from irregular or double-peaked narrow emission lines, blended objects, galaxy mergers, to potential dual AGN in close separation, BALs, and ERQs. However, our outlier detection scheme has also unveiled issues related to the data collection and processing pipelines. Predominantly, we find BGS outliers to be stars, misclassified by *Redrock* as galaxies.

This finding prompted the development of our own star model, following the same approach as for galaxies, but now applied to stellar spectra from the DESI MWS. We find good modeling quality without the PCA resid-

²² DESI 39627939041510701

²³ DESI 39627823501017204

²⁴ DESI 39633145246517940

²⁵ DESI 39632991718212824

²⁶ DESI 39633416341160166

²⁷ DESI 39633325958106929

²⁸ DESI 39633123197062964

²⁹ DESI 39627782380067362

³⁰ DESI 39633393184408234

³¹ DESI 39632956888715615

³² DESI 39633158374688229

³³ DESI 39633278931569179

³⁴ DESI 39632981354087949

³⁵ DESI 39627781683806700

³⁶ DESI 39633149726034475

³⁷ DESI 39633154058748211

³⁸ DESI 39633154041974595

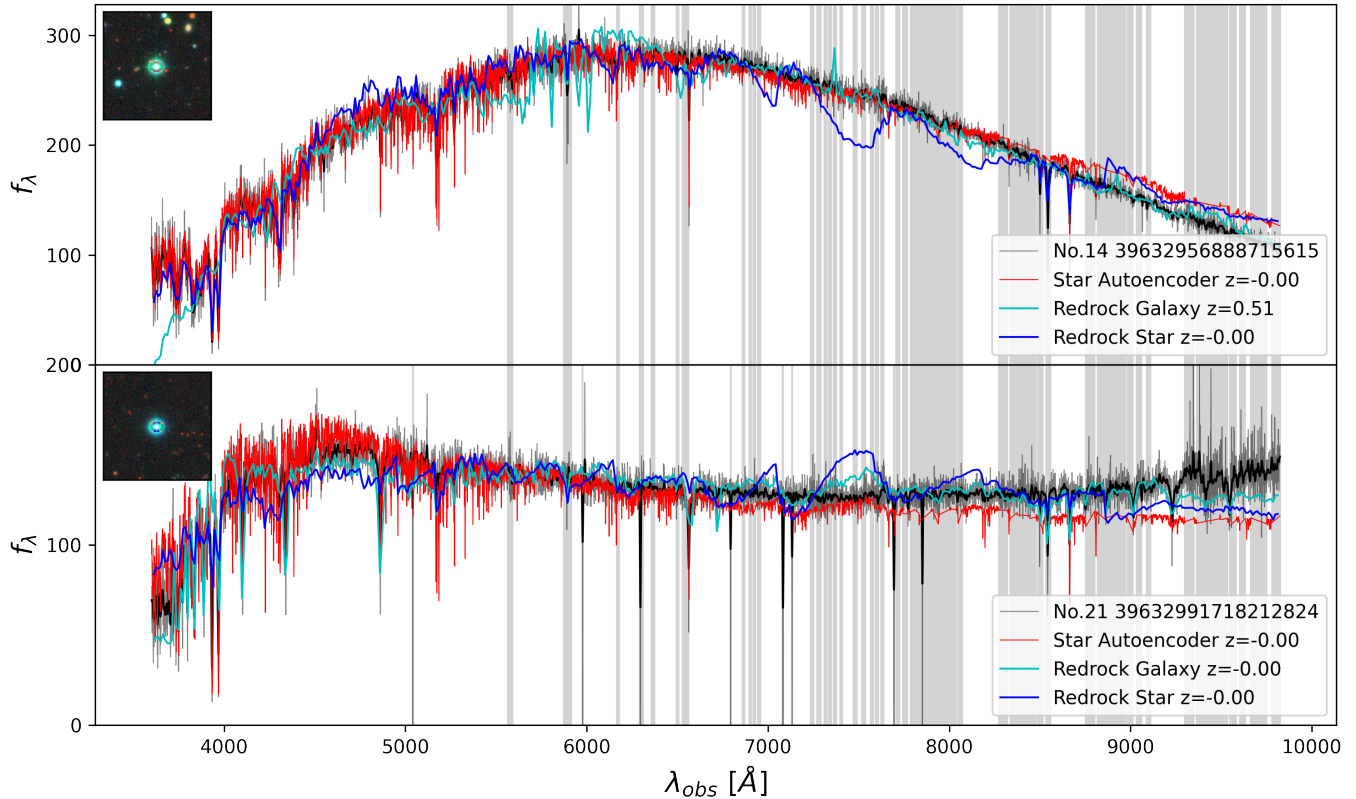


Figure 4. Comparison of observed spectra (black) and model fits (*Redrock* galaxy model (cyan), *Redrock* star model (blue), and our star autoencoder model (red)) for two example stars misclassified as galaxies by *Redrock*. Shaded regions indicate areas masked due to telluric contamination.

uals in the current *Redrock* PCA models. We also identified several more outliers that conform neither with our galaxy nor our star model. These are often blended sources, quasars, or spectra with calibration issues.

To facilitate further studies, we release the full catalog of galaxy and star probabilities and reconstruction qualities for all BGS objects at our code repository³⁹. The pre-trained autoencoder and normalizing flow models are also accessible with instructions at that URL.

As possible extensions of the work presented here, the pre-trained StarAE and StarNF models could be employed to identify unusual stars in the MWS sample for follow-up investigations. It is also entirely possible to create a star-galaxy classifier by running a spectrum through both of our pipelines and then compare the probabilities from each of the NFs to make classification decisions based on the relative likelihoods.

ACKNOWLEDGMENTS

We are grateful for the help of Michael Strauss in interpreting the weirdest spectra we discuss in this work.

This work was supported by the AI Accelerator program of the Schmidt Futures Foundation. The authors are pleased to acknowledge that the work reported on in this paper was substantially performed using the Princeton Research Computing resources at Princeton University, which is a consortium of groups led by the Princeton Institute for Computational Science and Engineering (PICSciE) and Office of Information Technology’s Research Computing.

Facilities: KPO:4m, APO:2.5m, Gaia, WISE

Software: `spender` (Melchior et al. 2022), `Pytorch` (Paszke et al. 2019), `corner` (Foreman-Mackey 2016), `umap` (Sainburg et al. 2021), `accelerate` (Gugger et al. 2022), `torchinterp1d`, `nflows` (Durkan et al. 2020), `NumPy` (Harris et al. 2020), `Astropy` (Astropy Collaboration et al. 2022), `Matplotlib` (Hunter 2007)

³⁹ <https://github.com/pmelchior/spender>

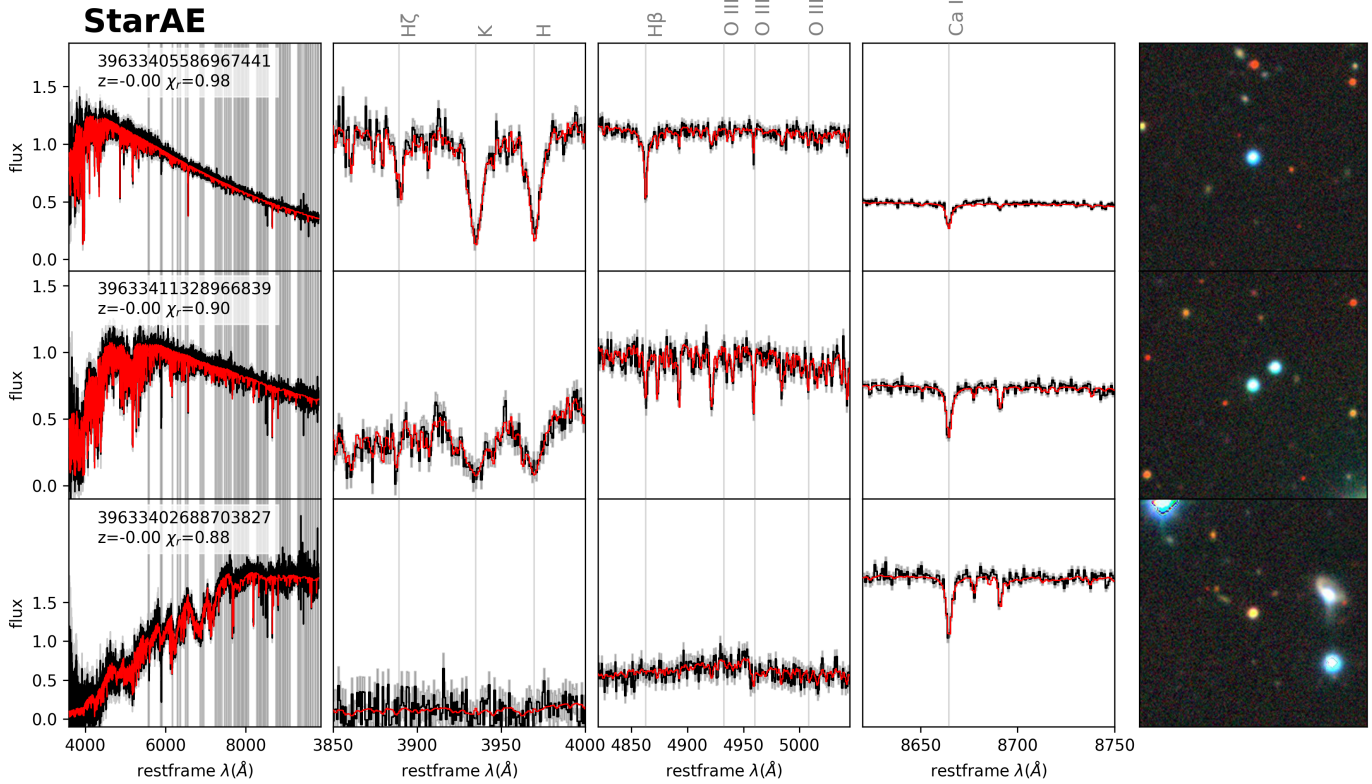


Figure 5. DESI MWS spectra (black) and their reconstructed models (red) from our star autoencoder. Panels as in Figure 2.

REFERENCES

- Astropy Collaboration, Price-Whelan, A. M., Lim, P. L., et al. 2022, *ApJ*, 935, 167, doi: [10.3847/1538-4357/ac7c74](https://doi.org/10.3847/1538-4357/ac7c74)
- Bellm, E. C., Kulkarni, S. R., Graham, M. J., et al. 2019, 018002, 1, doi: [10.1088/1538-3873/aaecbe](https://doi.org/10.1088/1538-3873/aaecbe)
- Best, P. N., & Heckman, T. M. 2012, *MNRAS*, 421, 1569, doi: [10.1111/j.1365-2966.2012.20414.x](https://doi.org/10.1111/j.1365-2966.2012.20414.x)
- Bolton, A. S., & Schlegel, D. J. 2010, *PASP*, 122, 248, doi: [10.1086/651008](https://doi.org/10.1086/651008)
- Chen, P. S., Yang, X. H., Liu, J. Y., & Shan, H. G. 2018, *AJ*, 155, 17, doi: [10.3847/1538-3881/aa988c](https://doi.org/10.3847/1538-3881/aa988c)
- Cooper, A. P., Kaposov, S. E., Allende Prieto, C., et al. 2023, *ApJ*, 947, 37, doi: [10.3847/1538-4357/acb3c0](https://doi.org/10.3847/1538-4357/acb3c0)
- De Propris, R., Conelice, C. J., Liske, J., et al. 2007, *ApJ*, 666, 212, doi: [10.1086/520488](https://doi.org/10.1086/520488)
- DESI Collaboration, Aghamousa, A., Aguilar, J., et al. 2016. <https://arxiv.org/abs/1611.00036>
- DESI Collaboration, Adame, A. G., Aguilar, J., et al. 2023a, arXiv e-prints, arXiv:2306.06308, doi: [10.48550/arXiv.2306.06308](https://doi.org/10.48550/arXiv.2306.06308)
- . 2023b, arXiv e-prints, arXiv:2306.06307, doi: [10.48550/arXiv.2306.06307](https://doi.org/10.48550/arXiv.2306.06307)
- Dey, A., Schlegel, D. J., Lang, D., et al. 2019, *AJ*, 157, 168, doi: [10.3847/1538-3881/ab089d](https://doi.org/10.3847/1538-3881/ab089d)
- Durkan, C., Bekasov, A., Murray, I., & Papamakarios, G. 2020, nflows: normalizing flows in PyTorch, v0.14, Zenodo, doi: [10.5281/zenodo.4296287](https://doi.org/10.5281/zenodo.4296287)
- Gaia* Collaboration, Brown, A. G. A., Vallenari, A., et al. 2018, *A&A*, 616, A1, doi: [10.1051/0004-6361/201833051](https://doi.org/10.1051/0004-6361/201833051)
- Foreman-Mackey, D. 2016, *The Journal of Open Source Software*, 1, 24, doi: [10.21105/joss.00024](https://doi.org/10.21105/joss.00024)
- Gaia* Collaboration, Brown, A. G. A., Vallenari, A., et al. 2021, *A&A*, 649, A1, doi: [10.1051/0004-6361/202039657](https://doi.org/10.1051/0004-6361/202039657)
- Graham, M. J., Kulkarni, S. R., Bellm, E. C., et al. 2019, *Publications of the Astronomical Society of the Pacific*, 131, 078001, doi: [10.1088/1538-3873/ab006c](https://doi.org/10.1088/1538-3873/ab006c)
- Gugger, S., Lysandre Debut, T. W., Schmid, P., Mueller, Z., & Mangrulkar, S. 2022, Accelerate: Training and inference at scale made simple, efficient and adaptable., <https://github.com/huggingface/accelerate>
- Guy, J., Bailey, S., Kremin, A., et al. 2023, *AJ*, 165, 144, doi: [10.3847/1538-3881/acb212](https://doi.org/10.3847/1538-3881/acb212)
- Hahn, C., Wilson, M. J., Ruiz-Macias, O., et al. 2023, *AJ*, 165, 253, doi: [10.3847/1538-3881/acccf8](https://doi.org/10.3847/1538-3881/acccf8)
- Hall, P. B., Anderson, S. F., Strauss, M. A., et al. 2002, *ApJS*, 141, 267, doi: [10.1086/340546](https://doi.org/10.1086/340546)

- Harris, C. R., Millman, K. J., van der Walt, S. J., et al. 2020, *Nature*, 585, 357, doi: [10.1038/s41586-020-2649-2](https://doi.org/10.1038/s41586-020-2649-2)
- Hunter, J. D. 2007, *Computing in Science & Engineering*, 9, 90, doi: [10.1109/MCSE.2007.55](https://doi.org/10.1109/MCSE.2007.55)
- Kim, D. C., Veilleux, S., & Sanders, D. B. 2002, *ApJS*, 143, 277, doi: [10.1086/343843](https://doi.org/10.1086/343843)
- Kozieł-Wierzbowska, D., Goyal, A., & Żywucka, N. 2020, *ApJS*, 247, 53, doi: [10.3847/1538-4365/ab63d3](https://doi.org/10.3847/1538-4365/ab63d3)
- Lai, T. S.-Y., Smith, J., Baba, S., Spoon, H. W., & Imanishi, M. 2020, *The Astrophysical Journal*, 905, 55
- Liang, Y., Melchior, P., Lu, S., Goulding, A., & Ward, C. 2023, arXiv e-prints, arXiv:2302.02496, doi: [10.48550/arXiv.2302.02496](https://doi.org/10.48550/arXiv.2302.02496)
- Lyke, B. W., Higley, A. N., McLane, J. N., et al. 2020, *ApJS*, 250, 8, doi: [10.3847/1538-4365/aba623](https://doi.org/10.3847/1538-4365/aba623)
- Melchior, P., Liang, Y., Hahn, C., & Goulding, A. 2022, arXiv e-prints, arXiv:2211.07890. <https://arxiv.org/abs/2211.07890>
- Nordin, J., Brinnel, V., Giomi, M., et al. 2020, *Transient Name Server Discovery Report*, 2020-624, 1
- Papamakarios, G., Pavlakou, T., & Murray, I. 2017, *Advances in neural information processing systems*, 30
- Paszke, A., Gross, S., Massa, F., et al. 2019, *Advances in neural information processing systems*, 32
- Ramazani, V. F., Lindfors, E., & Nilsson, K. 2017, *Astronomy & Astrophysics*, 608, A68
- Ross, N. P., Hamann, F., Zakamska, N. L., et al. 2015, *MNRAS*, 453, 3932, doi: [10.1093/mnras/stv1710](https://doi.org/10.1093/mnras/stv1710)
- Sainburg, T., McInnes, L., & Gentner, T. Q. 2021, *Neural Computation*, 33, 2881
- Shen, Y., Liu, X., Greene, J. E., & Strauss, M. A. 2011, *ApJ*, 735, 48, doi: [10.1088/0004-637X/735/1/48](https://doi.org/10.1088/0004-637X/735/1/48)
- Tabak, E. G., & Turner, C. V. 2013, *Communications on Pure and Applied Mathematics*, 66, 145
- Tabak, E. G., & Vanden-Eijnden, E. 2010, *Communications in Mathematical Sciences*, 8, 217
- Véron-Cetty, M.-P., & Véron, P. 2010, *Astronomy & Astrophysics*, 518, A10
- York, D. G., Adelman, J., Anderson Jr, J. E., et al. 2000, *The Astronomical Journal*, 120, 1579
- Zakamska, N. L., Hamann, F., Pâris, I., et al. 2016, *MNRAS*, 459, 3144, doi: [10.1093/mnras/stw718](https://doi.org/10.1093/mnras/stw718)